

Back-action supercurrent diodes

Daniel Margineda,^{1,*} Alessandro Crippa,¹ Elia Strambini,^{1,†} Yuri Fukaya,² Maria Teresa Mercaldo,³ Carmine Ortix,³ Mario Cuoco,^{2,‡} and Francesco Giazotto^{1,§}

¹*NEST Istituto Nanoscienze-CNR and Scuola Normale Superiore, I-56127, Pisa, Italy*

²*SPIN-CNR, I-84084 Fisciano (SA), Italy*

³*Dipartimento di Fisica “E. R. Caianiello”, Università di Salerno, I-84084 Fisciano (SA), Italy*

Back-action refers to a response that retro-acts on a system to tailor its properties with respect to an external stimulus. This self-induced effect generally belongs to both the natural and technological realm, ranging from neural networks [1] to optics [2] and electronic circuitry [3]. In electronics, back-action mechanisms are at the heart of many classes of devices such as amplifiers, oscillators, and sensors [4]. Here, we demonstrate that back-action can be successfully exploited to achieve *non-reciprocal* transport in superconducting circuits. Our device realizes a supercurrent diode, since the dissipationless current flows in one direction whereas dissipative transport occurs in the opposite direction. Supercurrent diodes presented so far rely on magnetic elements or vortices to mediate charge transport or external magnetic fields to break time-reversal symmetry [5–9]. In our implementation, back-action solely turns a conventional reciprocal superconducting weak link with no asymmetry between the current bias directions into a diode, where the critical current amplitude depends on the bias sign. The self-interaction of the supercurrent with the device stems from the gate tunability of the critical current, which uniquely promotes up to $\sim 88\%$ of magnetic field-free signal rectification and diode functionality with selectable polarity. The concept we introduce is very general and can be applied directly to a large variety of devices, thereby opening novel functionalities in superconducting electronics.

Introduction

Control of dissipationless transport is a core challenge for superconducting electronics and it is at the heart of several applications including both classical [10] and quantum [11] computation. The flow of dissipationless current relies on macroscopic quantum coherence and exploits the phase difference between spatially separated superconducting condensates. The resulting supercurrent cannot exceed a critical amplitude, I_c , above which the superconductor turns into the normal state. In analogy with the semiconducting counterpart, the superconducting diode effect refers to dissipationless current flowing in one direction (+) while the current is driven by dissipative carriers in the opposite direction (−), thereby leading to asymmetric amplitudes of the critical currents $I_c^+ \neq |I_c^-|$.

The discovery and design of quantum materials and platforms suitable for nonreciprocal superconducting transport have been developed around the fundamental requirement of realizing the lack of inversion and time-reversal symmetries [5, 6, 12–14]. This condition is, for instance, realized in systems that are naturally equipped with symmetry-breaking crystalline potentials and magnetic interactions, as with non-centrosymmetric or magnetic materials [7, 15, 16] and related heterostructures [17]. Alternatively, several implementations exploit external magnetic fields [5, 18, 19] leading to symmetry-breaking configurations, which yield nonreciprocal superconducting transport. Hence, the current paradigm for superconducting diodes either relies on internal mechanisms [20–22], or on suitably designed external sources to

break time and spatial symmetry [23–25].

Here, we propose a completely new paradigm within nonreciprocal superconducting transport that arises from the back-action of the supercurrent with itself in a fully symmetric superconducting wire. The idea of exploiting a back-action mechanism not linked to internal or external sources of symmetry breaking aims at a general design principle suitable for several superconducting platforms. We demonstrate how to achieve a back-action on the supercurrent amplitude via an applied gate voltage to a superconducting weak link. This self-induced effect provides a fundamental path to rectify the supercurrent, thereby leading to a superconducting diode effect with tunable and high rectification efficiency. The back-action of the supercurrent on the effective gate voltage relies on a control resistor in series with the Josephson element. The gate voltage modifies the supercurrent, which in turn alters the effective gate voltage experienced by the weak link, thereby realizing a retroaction. Our findings set out a general paradigm for the design of all-electrical and magnetic field-free supercurrent diodes.

Results

Device concept. The magnitude of the dissipationless supercurrent I through a Josephson element is entangled to the superconducting phase difference ϕ across the junction via the so-called current-phase relation $I(\phi)$. In its simplest form, it reads $I(\phi) = I_c \sin(\phi)$, and in generic reciprocal junctions it is an odd 2π -periodic function of ϕ . From the functional form above, it follows immediately the reciprocity of the two critical currents, as depicted in the bottom left sketch of Fig. 1: $I_c^+ = \max(I(\phi)) = |I_c^-| = |\min(I(\phi))| = I_c$. The reciprocity can be violated in systems that concomitantly break inversion and time-reversal symmetry either intrinsically or using applied fields. The concept of a back-action

* d.margineda@nanogune.eu, present address: CIC nanoGUNE BRTA, E-20018 Donostia-San Sebastián, Spain.

† elia.strambini@nano.cnr.it

‡ mario.cuoco@spin.cnr.it

§ francesco.giazotto@sns.it

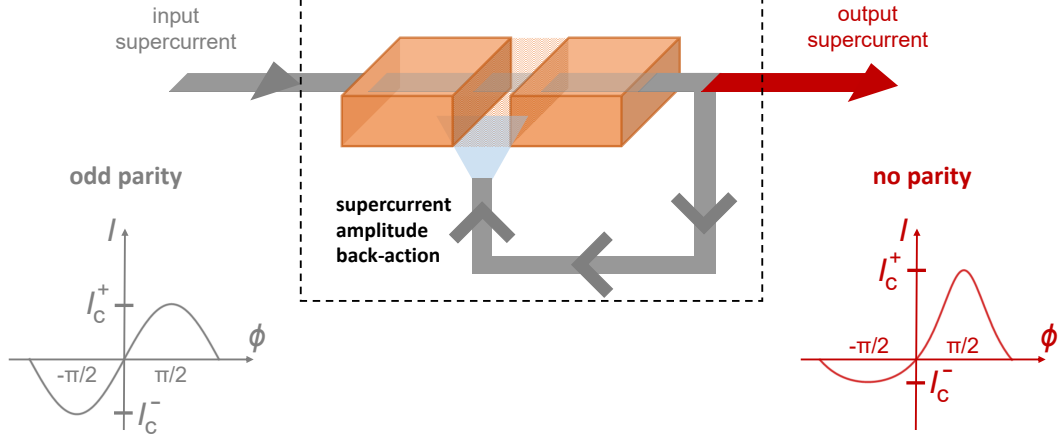


FIG. 1. **Principle of supercurrent diode effect by supercurrent amplitude back-action.** Cartoon of a generic weak link with two superconducting banks (orange) separated by an element with weaker superconductivity (orange with texture). A period of the current-phase relation of the input current injected from the left lead is shown, and it is odd-in- ϕ . The supercurrent coming out from the right lead retroacts on the weak link itself, thereby generating an output supercurrent with no defined parity on ϕ . The odd parity of the input current-phase relation dictates $I_c^+ = |I_c^-|$, while the back-action results in an output supercurrent without defined parity in ϕ , so that $I_c^+ \neq |I_c^-|$. See the main text for a model of the back-action mechanism.

supercurrent diode instead relies on a modulation of I_c induced by the flowing current I . For the sake of simplicity, we assume a linear modulation of the form $I_c = I_c^0 + \alpha I$, where $-1 < \alpha < 1$ represents the back-action strength, and I_c^0 is the critical current in the absence of back-action ($\alpha = 0$). Other monotonic functions $I_c(I)$ bring similar conclusions, provided that I_c and ϕ are factorized in the current-phase relation, i.e., $I(\phi) = f(I)g(\phi)$. Solving the self-consistent equation $I = (I_c^0 + \alpha I) \sin \phi$ yields $I(\phi) = I_c^0 \frac{\sin \phi}{1 - \alpha \sin \phi}$, which is a functional form with a non-defined parity, as sketched in the bottom right of Fig 1. It is straightforward to show that the above function is non-reciprocal, with $|I_c^\pm| = \frac{I_c^0}{1 \mp \alpha}$ and rectification efficiency $\eta \equiv (I_c^+ - |I_c^-|)/(I_c^+ + |I_c^-|) = \alpha$. Hence, in the limit of $|\alpha| \simeq 1$ an ideal rectification can be achieved. The model so far described, though very minimal, captures the essential features of back-action: i) parity violation of the current-phase relation, ii) zero spontaneous supercurrent [i.e., $I(0) = 0$], and iii) nonreciprocal supercurrent and tunable rectification amplitude (See Supplementary Note for a formal discussion).

Implementation of a back-action supercurrent diode. We now turn to the physical realization of the back-action mechanism. First, we introduce the circuitry that allows the operation of a generic *gate-tunable* Josephson junction as a highly efficient supercurrent diode. Later, we present the sample of the experiment and characterize its performance.

Figure 2a shows the schematic of the current-biased setup. The cross represents a weak link whose critical current is mea-

sured by sweeping the current bias I till the transition to the normal state is detected by a finite voltage drop V across the weak link. Red and blue bias currents correspond to positive and negative sweep directions, respectively. A third control terminal tunes the critical current via a voltage source at V_g^0 . The feedback network consists of a control resistor R_c embedded between the weak link and the ground. Thus, the bias current I lifts upward or downward the weak link potential according to its direction resulting in a polarity-dependent gate voltage, $V_g = V_g^0 - IR_c$.

Figure 2b illustrates the diode principle: at a voltage bias V_g^0 for which I_c depends on the gate voltage (i.e., $\partial I_c / \partial V_g \neq 0$), the critical current for a positive bias current I_c^+ (red) differs in modulus from the critical current for a negative bias current $|I_c^-|$ (blue), thereby resulting in $I_c^+ \neq |I_c^-|$. As shown below, the strength of the non-reciprocity depends both on the magnitude of R_c and on $\partial I_c / \partial V_g$, which we shall refer to as transconductance g_m .

This scheme is implemented with a nanosized constriction of a superconducting stripe patterned from a niobium (Nb) thin film. Such type of weak link, called Dayem bridge, has shown a reduction of the critical currents up to full suppression under the action of a strong gating effect [26–28]. Next to other metallic platforms, such as superconducting nanowires [29–31], superconductor-normal metal-superconductor Josephson junctions [32, 33], and hybrid semiconductor-superconductor weak links [34–39], Dayem bridges typically display larger critical currents, often reaching fractions of mA, which translate into higher transconductance g_m and, ultimately, in improved diode efficiencies. A

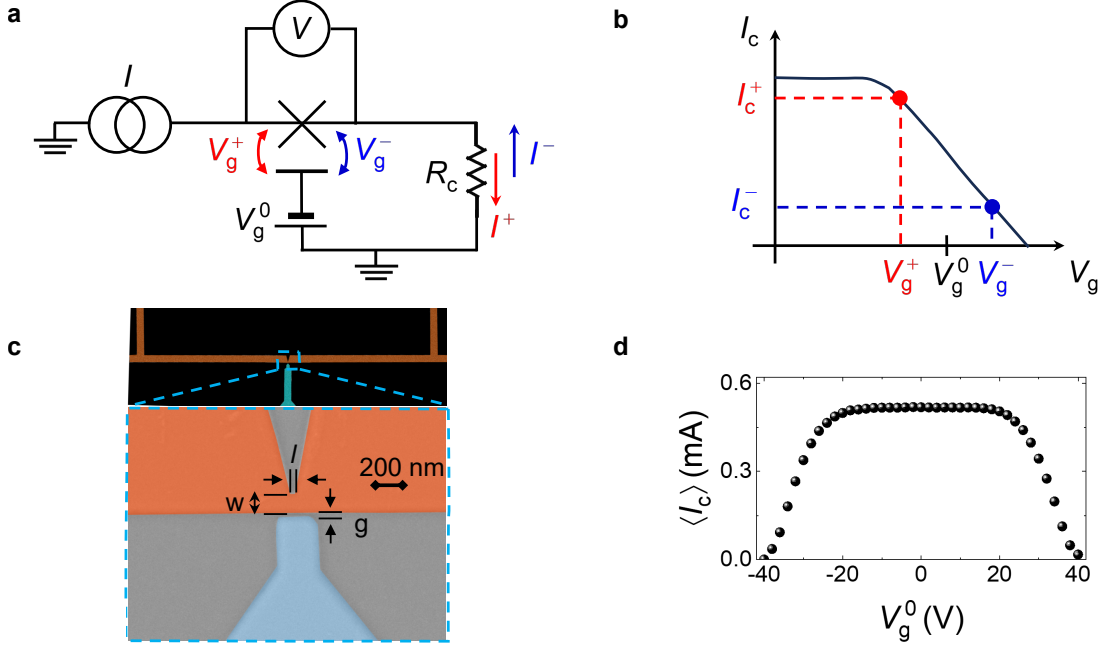


FIG. 2. **Setup for the back-action supercurrent diode.** **a**, Circuit schematic to realize a supercurrent diode by back-action mechanism. The cross represents a weak link measured in a current-biased (I) setup by monitoring the voltage drop across it (V). A gate electrode at nominal voltage V_g^0 tunes the critical current of the weak link nearby. A control resistor in series, R_c , modifies V_g^0 into $V_g = V_g^0 - IR_c$, depending on the sign of the current bias I . **b**, Effect of the circuitry presented in **a** on a representative critical current vs. gate voltage trace. At a certain gate voltage bias V_g^0 , the positive critical current I_c^+ (red dot) at V_g^+ differs from the negative critical current I_c^- (blue dot) at V_g^- resulting in a finite diode effect, i.e., $I_c^+ \neq |I_c^-|$. **c**, Scanning electron micrograph of a niobium (Nb) strip (orange) with a nanoconstriction (characteristic dimensions $l \sim 80$ nm and $w \sim 180$ nm) to implement the superconducting weak link. The gate voltage V_g^0 is applied through a side gate (light blue) located at distance $g \sim 50$ nm. **d**, Experimental gate voltage dependence of the average critical current $\langle I_c \rangle = (I_c^+ + |I_c^-|)/2$ recorded at $T = 1$ K with $R_c = 2$ k Ω .

micrograph of a typical diode sample is shown in Fig. 2c. A constant-thickness strip of niobium (orange) is interrupted by a constriction of length $l \sim 80$ nm and width $w \sim 180$ nm. A side electrode (cyan colored) is placed at a distance $g \sim 50$ nm. See Ref. [40] and Methods for basic electrical characterizations and further fabrication details. Figure 2d displays the modulation of the average critical current $\langle I_c \rangle = (I_c^+ + |I_c^-|)/2$ as a function of the gate bias V_g^0 at $T \simeq 1$ K. As in former experiments, a plateau is followed by a bipolar decay of the critical current, which is roughly linear in gate voltage V_g^0 up to its full suppression at $|V_g^0| \simeq 40$ V. The critical current modulation occurs along with a tiny gate-delivered leakage current of a few pA at the onset of the damp of I_c up to a few nA at full suppression (see Supplementary Figure 1).

Figure 3a-e demonstrates that non-reciprocity of the critical currents emerges for finite gate voltages via a series resistor, and can be easily tuned in amplitude. We show the switching currents while sweeping the biasing current from zero to positive values (I_c^+ , blue dots) or from zero to negative values ($|I_c^-|$, orange dots) as a function of the nominal gate voltage V_g^0 . The control resistor R_c ranges from 2 k Ω to 22 k Ω . As R_c increases, the data sets of positive and negative critical currents move apart. The nonreciprocal component of the critical

current, $\Delta I_c = I_c^+ - |I_c^-|$, is plotted in Fig. 3f-j for the same values of R_c . The curves are odd-in- V_g^0 but nonmonotonic, with peaks at $\simeq \pm 32$ V that increase in magnitude with R_c .

To further confirm the role of the control resistor in driving the supercurrent non-reciprocity, we display the critical currents with respect to the gate voltage normalized by the back-action contribution in Fig. 3k. By defining $V_{g,c}^\pm = V_g^0 - I_c^\pm R_c$, positive and negative critical currents become identical within the experimental accuracy (see also Supplementary Figure 2).

As previously outlined, the transconductance g_m plays a key role in the diode performance. Figure 3l shows the evolution of $g_m = \partial \langle I_c \rangle / \partial V_g^0$ as a function of the gate voltage for $R_c = 2$ k Ω and different bath temperatures (see also Supplementary Figure 3). g_m exhibits a peak at $|V_g^0| \simeq 32$ V and can be tuned by the temperature (see the inset for a maximum of g_m at different temperatures). Its decrease at high T can be ascribed to temperature-induced decay of the critical current [40].

Finally, it may be convenient to estimate the strength of the back-action. For the toy model developed in the first section, the parameter α weights the dependence of the critical current on the supercurrent and the rectification. The analogous quantity in our experiment is $-R_c g_m$, a dimensionless parameter that quantifies dI_c/dI . Figure 3m shows the rectification

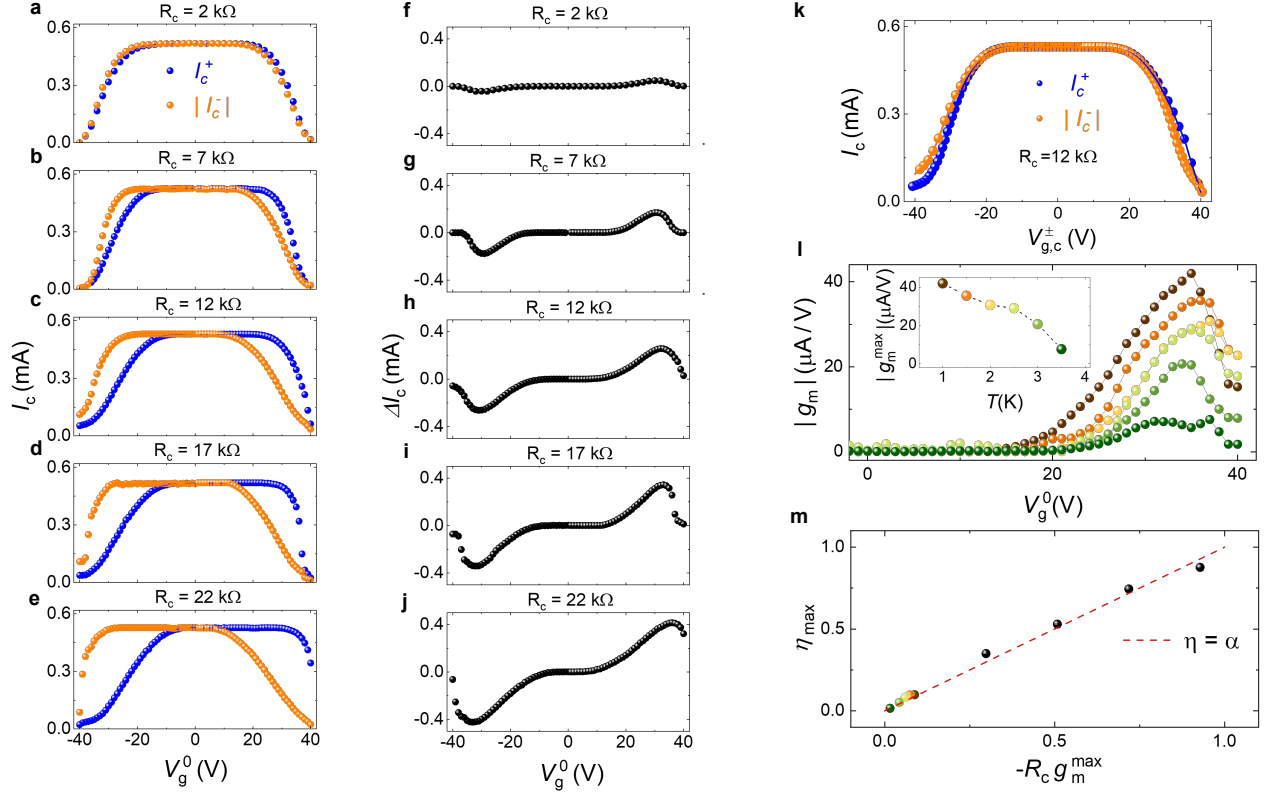


FIG. 3. Back-action supercurrent diode characterization. **a-e**, Gate voltage dependence of the switching current for positive I_c^+ (blue dots) and negative $|I_c^-|$ (orange dots) bias current for different values of the control resistor R_c . The diode effect results in $I_c^+ \neq |I_c^-|$ and is enhanced by the increase of R_c from 2 kΩ to 22 kΩ. **f-j**, $\Delta I_c = I_c^+ - |I_c^-|$ as a function of V_g^0 obtained from the data in **a-e**. **k**, Quasi-symmetric behavior the critical currents obtained by normalizing the gate voltage with the back-action contribution, $V_{g,c}^\pm = V_g^0 - I_c^\pm R_c$ for $R_c = 12$ kΩ. Similar plots for all the configurations (variation of R_c or temperature) are in Supplementary Figure 2. **l**, Transconductance $g_m = \partial \langle I_c \rangle / \partial V_g^0$ as a function of gate voltage V_g^0 for different bath temperatures T . Color code is given in the inset where the maximum transconductance g_m^{\max} versus temperature T is plotted. **m** Diode rectification efficiency η evaluated at its maximum value (η_{\max}) as a function of $-R_c g_m^{\max}$. Black dots are measured at $T = 1$ K by varying R_c , while the color dots are obtained via tuning g_m by temperature. Data converge to null rectification, thereby validating the back-action at the origin of the supercurrent diode effect. The red dashed line is a reference to the basic model of linear dependence of the critical current on the supercurrent amplitude, which yields $-R_c g_m = d\langle I_c \rangle / dI = \alpha$.

efficiency evaluated at its maximum η_{\max} as a function of $-R_c g_m^{\max}$. A linear trend is observed, as in the model where $\eta = \alpha$ (see Supplementary Figure 4). Black dots are obtained at 1 K by changing the control resistor R_c , whereas the data next to the axes origin are measured by tuning the transconductance g_m by changing the bath temperature (color code as in Fig. 3l). Remarkably, our diode reaches a quasi-ideal rectification efficiency, $\eta_{\max} \simeq 88\%$ for $R_c = 22$ kΩ at $T = 1$ K.

We now demonstrate possible applications of our device as a supercurrent diode with tunable polarity and as a half-wave rectifier. Figure 4a presents a color plot of $I - V$ characteristics as a function of the gate voltage V_g^0 for a control resistor $R_c = 22$ kΩ. The yellow vertical lines define three working regimes depending on the gate voltage: no sizable rectification, marked by a conventional (reciprocal) Josephson junction symbol; the supercurrent diode regimes with dominant negative or positive supercurrent, corresponding to the left and right region of the plot respectively. Therefore, the system op-

erates as a quasi-ideal supercurrent diode whose polarity can be changed by simply inverting the sign of the gate voltage.

In the right quadrant of Fig. 4a, the weak link is predominantly superconducting with a positive bias current but dissipative with a negative bias current. This opens the possibility of exploiting the diode as a half-wave rectifier for AC currents. In principle, this idea holds for supercurrent diodes with any rectification efficiency, till the applied current amplitude lies between $|I_c^-|$ and I_c^+ . However, having a quasi-ideal rectification efficiency, like in our case, widens the range of amplitudes of the injected AC current to be rectified, which greatly relaxes the limitations in applications. Figure 4b shows the half-wave rectified voltage output $V(t)$ (black trace) and the applied current $I(t)$ of amplitude 0.4 mA and frequency 0.87 Hz (red sinusoidal signal) measured at $V_g^0 = 33$ V for $R_c = 12$ kΩ. A zero-voltage output occurs for $I(t) > 0$ (superconducting state, gray bands), while the system follows the applied current signal for $I(t) < 0$ (dissipative state, white bands).

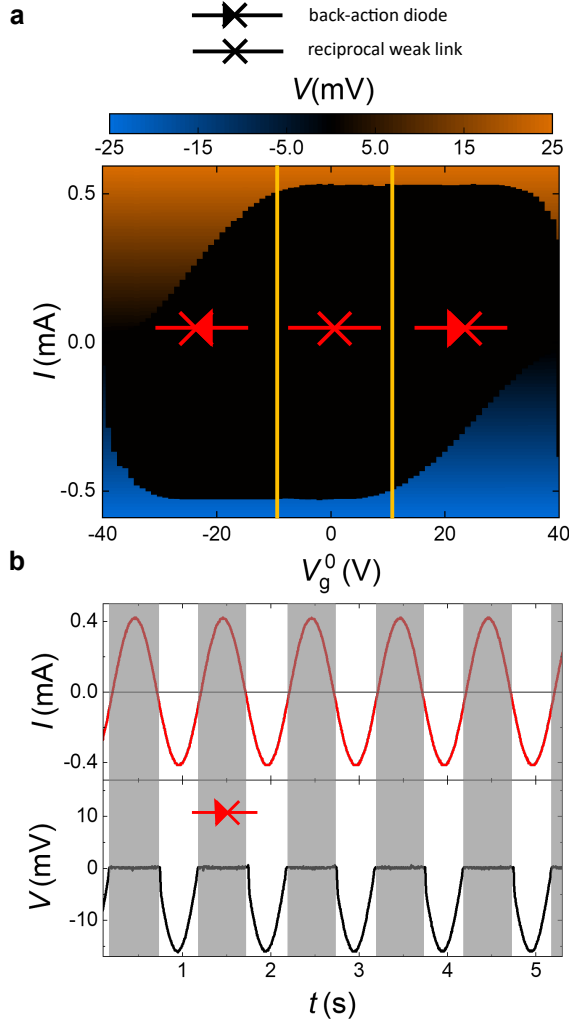


FIG. 4. **Diode polarity tunability and half-wave rectification.** **a**, Contour plot of the voltage drop V versus biasing current I and gate voltage V_g^0 measured at 1K for $R_c = 22 \text{ k}\Omega$. Yellow lines mark three regions: the central one, where reciprocal transport takes place and the device behaves as a Josephson reciprocal element (cross symbol), and two external areas beyond the lines, where the polarity-dependent diode behavior is achieved. At $|V_g^0| \simeq 32 \text{ V}$, very large rectification efficiency ($\eta \simeq 88 \%$) is achieved. **b**, Half-wave rectifier of the input AC current (upper panel). At $V_g^0 = 33 \text{ V}$ and for $R_c = 12 \text{ k}\Omega$, the output voltage follows the current only in the negative semi-period (i.e., when the weak link is *dissipative*, white bands); on the contrary, $V = 0$ in the positive semi-period of I when the Dayem bridge is superconducting (grey bands). White and grey bands slightly differ in width as the rectification is not ideal. The AC biasing current has an amplitude of 0.4 mA and frequency of 0.87 Hz.

Conclusions

In summary, we have proposed and implemented a supercurrent back-action diode. To date, most efforts devoted to lifting the odd parity in the current-phase relation in superconducting weak links rely on magnetic exchange interactions [41, 42] and magnetic fields in combination with sizable spin-orbit

coupling [37, 43–45], or nonequilibrium conditions [46]. Instead, the original class of diodes presented here counts on the self-induced effect of the supercurrent amplitude to break the parity condition. Though intrinsically reciprocal, supercurrent transport across the metallic weak link is made nonreciprocal by the retroaction of the bias current on the weak link itself. This results in a tuning of the critical current by a gate voltage sensitive to the current polarity. The rectification efficiency is easily tunable and can be boosted to nearly ideal values. Such reduction of fabrication complexity joined to the absence of magnetic fields represents a clear asset for scalability and integration with other superconducting devices, making our diode attractive for next-generation superconducting electronics.

The back-action mechanism based on the current bias can be applied to other gate-tunable superconducting systems, such as hybrid semiconducting-superconducting Josephson field-effect transistors. More generally, we expect the back-action supercurrent diode to be implemented on all the superconducting platforms adjustable by other control knobs such as phonon-controlled Josephson junctions [47, 48], flux-retroacted superconducting quantum interference devices [49], or quasiparticle injection-driven superconducting transistors [50–54]. Finally, new functionalities are expected beyond the linear back-action approximation used in this work for rectification improvements or multi-valued circuits. Thus, our results pave the way for designing a new class of superconducting technologies with tunable and enhanced performances.

Methods

Sample fabrication. Nb strips and constrictions are patterned by e-beam lithography on AR-P 679.04 (PMMA) resist. PMMA residuals are removed by O_2 -plasma etching after developing. Nb thin films of 25 nm thickness were deposited by sputtering at a base pressure of 2×10^{-8} Torr in a 4 mTorr Ar (6N purity) atmosphere and liftoff by AR-P 600.71 remover.

Transport measurements. Transport measurements were carried out in filtered (two-stage RC and π filters) cryogen-free ^3He - ^4He dilution refrigerators by a standard 4-wire technique. DC current-voltage characteristics were measured by sweeping a low-noise current bias positively and negatively, and by measuring the voltage drop occurring across the weak links with a room-temperature low-noise pre-amplifier. The switching currents and error bars were obtained from 10–20 reiterations of the IV curves, and their accuracy is mostly given by the current step set to $\Delta I < 0.002 I_c(V_g^0 = 0)$, where I_c is the switching current of the Nb nanobridge. Joule heating in the system is minimized by automatically switching the current off once the device turns into the normal state. A delay between sweeps was optimized to keep the stability of the fridge temperature lower than 50 mK. Furthermore, no changes in the switching currents (up to the accuracy given by the standard deviation) were observed in

different cooling cycles, by changing the order of the sweeps, or by adding an extra delay in the acquisition protocol, thereby concluding that hysteretic behavior or local heating is negligible. The gate-nanobridge current I_g was acquired by using a low-noise voltage source and a 10^{-11} A/V-gain low-noise current amplifier in a two-wire configuration.

Data availability

The data that support the findings of this study are available from the corresponding author upon reasonable request.

-
- [1] Y. LeCun, Y. Bengio, and G. Hinton, Deep learning, *Nature* **521**, 436–444 (2015).
- [2] M. L. Juan, R. Gordon, Y. Pang, F. Eftekhari, and R. Quidant, Self-induced back-action optical trapping of dielectric nanoparticles, *Nat. Phys.* **5**, 915–919 (2009).
- [3] P. Horowitz, W. Hill, and I. Robinson, The art of electronics, Vol. 2 (Cambridge University Press Cambridge, 1989).
- [4] S. Kal, Basic electronics: Devices, circuits and IT fundamentals (PHI Learning Pvt. Ltd., 2009).
- [5] F. Ando, Y. Miyasaka, T. Li, J. Ishizuka, T. Arakawa, Y. Shiota, T. Moriyama, Y. Yanase, and T. Ono, Observation of superconducting diode effect, *Nature* **584**, 373–376 (2020).
- [6] H. Wu, Y. Wang, Y. Xu, P. K. Sivakumar, C. Pasco, U. Filippozzi, S. S. P. Parkin, Y.-J. Zeng, T. McQueen, and M. N. Ali, The field-free josephson diode in a van der waals heterostructure, *Nature* **604**, 653–656 (2022).
- [7] M. Trahms, L. Melischek, J. F. Steiner, B. Mahendru, I. Tamir, N. Bogdanoff, O. Peters, G. Reece, C. B. Winkelmann, F. von Oppen, and K. J. Franke, Diode effect in Josephson junctions with a single magnetic atom, *Nature* **615**, 628–633 (2023).
- [8] T. Golod and V. M. Krasnov, Demonstration of a superconducting diode-with-memory, operational at zero magnetic field with switchable nonreciprocity, *Nat. Commun.* **13**, 3658 (2022).
- [9] A. Gutfreund, H. Matsuki, V. Plastovets, A. Noah, L. Gorzawski, N. Fridman, G. Yang, A. Buzdin, O. Millo, J. W. Robinson, et al., Direct observation of a superconducting vortex diode, *Nat. Commun.* **14**, 1630 (2023).
- [10] K. K. Likharev and V. K. Semenov, RSFQ logic/memory family: a new josephson-junction technology for sub-terahertz-clock-frequency digital systems, *IEEE Trans. Appl. Supercond.* **1**, 3–28 (1991).
- [11] J. Clarke and F. K. Wilhelm, Superconducting quantum bits, *Nature* **453**, 1031–1042 (2008).
- [12] K.-R. Jeon, J.-K. Kim, J. Yoon, J.-C. Jeon, H. Han, A. Cottet, T. Kontos, and S. S. P. Parkin, Zero-field polarity-reversible josephson supercurrent diodes enabled by a proximity-magnetized Pt barrier, *Nat. Mater.* **21**, 1008–1013 (2022).
- [13] C. Baumgartner, L. Fuchs, A. Costa, S. Reinhardt, S. Gronin, G. C. Gardner, T. Lindemann, M. J. Manfra, P. E. Faria Junior, D. Kochan, J. Fabian, N. Paradiso, and C. Strunk, Supercurrent rectification and magnetochiral effects in symmetric Josephson junctions, *Nat. Nanotechnol.* **17**, 39–44 (2022).
- [14] L. Bauriedl, C. Bäuml, L. Fuchs, C. Baumgartner, N. Paulik, J. M. Bauer, K.-Q. Lin, J. M. Lupton, T. Taniguchi, K. Watanabe, C. Strunk, and N. Paradiso, Supercurrent diode effect and magnetochiral anisotropy in few-layer NbSe₂, *Nat. Commun.* **13**, 4266 (2022).
- [15] H. Narita, J. Ishizuka, R. Kawarazaki, D. Kan, Y. Shiota, T. Moriyama, Y. Shimakawa, A. V. Ognev, A. S. Samardak, Y. Yanase, and T. Ono, Field-free superconducting diode effect in noncentrosymmetric superconductor/ferromagnet multilayers, *Nat. Nanotechnol.* **17**, 823–828 (2022).
- [16] J.-X. Lin, P. Siriviboon, H. D. Scammell, S. Liu, D. Rhodes, K. Watanabe, T. Taniguchi, J. Hone, M. S. Scheurer, and J. I. A. Li, Zero-field superconducting diode effect in small-twist-angle trilayer graphene, *Nat. Phys.* **18**, 1221–1227 (2022).
- [17] M. Nadeem, M. S. Fuhrer, and X. Wang, The superconducting diode effect, *Nat. Rev. Phys.* **5**, 558–577 (2023).
- [18] V. M. Edelstein, Magnetoelectric effect in polar superconductors, *Phys. Rev. Lett.* **75**, 2004–2007 (1995).
- [19] R. Wakatsuki, Y. Saito, S. Hoshino, Y. M. Itahashi, T. Ideue, M. Ezawa, Y. Iwasa, and N. Nagaosa, Nonreciprocal charge transport in noncentrosymmetric superconductors, *Sci. Adv.* **3**, e1602390 (2017).
- [20] A. Daido and Y. Yanase, Superconducting diode effect and nonreciprocal transition lines, *Phys. Rev. B* **106**, 205206 (2022).
- [21] J. J. He, Y. Tanaka, and N. Nagaosa, A phenomenological theory of superconductor diodes, *New J. Phys.* **24**, 053014 (2022).
- [22] S. Ilić and F. S. Bergeret, Theory of the supercurrent diode effect in Rashba superconductors with arbitrary disorder, *Phys. Rev. Lett.* **128**, 177001 (2022).
- [23] D. Suri, A. Kamra, T. N. G. Meier, M. Kronseder, W. Belzig, C. H. Back, and C. Strunk, Non-reciprocity of vortex-limited critical current in conventional superconducting micro-bridges, *Appl. Phys. Lett.* **121**, 102601 (2022).
- [24] Y. Hou, F. Nichele, H. Chi, A. Lodesani, Y. Wu, M. F. Ritter, D. Z. Haxell, M. Davydova, S. Ilić, O. Glezakou-Elbert, A. Varambally, F. S. Bergeret, A. Kamra, L. Fu, P. A. Lee, and J. S. Moodera, Ubiquitous Superconducting Diode Effect in Superconductor Thin Films, *Phys. Rev. Lett.* **131**, 027001 (2023).
- [25] A. Sundaresh, J. I. Väyrynen, Y. Lyanda-Geller, and L. P. Rokhinson, Diamagnetic mechanism of critical current non-reciprocity in multilayered superconductors, *Nat. Commun.* **14**, 1628 (2023).
- [26] F. Paolucci, G. De Simoni, P. Solinas, E. Strambini, N. Ligato, P. Virtanen, A. Braggio, and F. Giazotto, Magnetotransport Experiments on Fully Metallic Superconducting Dayem-Bridge Field-Effect Transistors, *Phys. Rev. Appl.* **11**, 024061 (2019).
- [27] C. Puglia, G. De Simoni, and F. Giazotto, Electrostatic Control of Phase Slips in Ti Josephson Nanotransistors, *Phys. Rev. Appl.* **13**, 054026 (2020).
- [28] F. Paolucci, F. Crisá, G. De Simoni, L. Bours, C. Puglia, E. Strambini, S. Roddaro, and F. Giazotto, Electrostatic Field-Driven Supercurrent Suppression in Ionic-Gated Metallic Superconducting Nanotransistors, *Nano Letters* **21**, 10309–10314 (2021).
- [29] G. De Simoni, F. Paolucci, P. Solinas, E. Strambini, and F. Giazotto, Metallic supercurrent field-effect transistor, *Nat. Nanotechnol.* **13**, 802–805 (2018).
- [30] L. D. Alegria, C. G. L. Böttcher, A. K. Saydjari, A. T. Pierce, S. H. Lee, S. P. Harvey, U. Vool, and A. Yacoby, High-energy quasiparticle injection into mesoscopic superconductors, *Nat. Nanotechnol.* **16**, 404–408 (2021).
- [31] M. F. Ritter, N. Crescini, D. Z. Haxell, M. Hinderling, H. Riel, C. Bruder, A. Fuhrer, and F. Nichele, Out-of-equilibrium phonons in gated superconducting switches, *Nat. Electron.* **5**, 71–77 (2022).
- [32] G. De Simoni, F. Paolucci, C. Puglia, and F. Giazotto, Josephson Field-Effect Transistors Based on All-Metallic Al/Cu/Al Proximity Nanojunctions, *ACS Nano* **13**, 7871–7876 (2019).

- [33] J. Basset, O. Stanisavljević, M. Kuzmanović, J. Gabelli, C. H. L. Quay, J. Estève, and M. Aprili, Gate-assisted phase fluctuations in all-metallic Josephson junctions, *Phys. Rev. Res.* **3**, 043169 (2021).
- [34] T. Akazaki, H. Takayanagi, J. Nitta, and T. Enoki, A Josephson field effect transistor using an InAs-inserted-channel $\text{In}_{0.52}\text{Al}_{0.48}\text{As}/\text{In}_{0.53}\text{Ga}_{0.47}\text{As}$ inverted modulation-doped structure, *Appl. Phys. Lett.* **68**, 418–420 (1996).
- [35] Y.-J. Doh, J. A. van Dam, A. L. Roest, E. P. A. M. Bakkers, L. P. Kouwenhoven, and S. De Franceschi, Tunable supercurrent through semiconductor nanowires, *Science* **309**, 272–275 (2005).
- [36] P. Jarillo-Herrero, J. A. van Dam, and L. P. Kouwenhoven, Quantum supercurrent transistors in carbon nanotubes, *Nature* **439**, 953–956 (2006).
- [37] J. A. van Dam, Y. V. Nazarov, E. P. A. M. Bakkers, S. De Franceschi, and L. P. Kouwenhoven, Supercurrent reversal in quantum dots, *Nature* **442**, 667–670 (2006).
- [38] J. Xiang, A. Vidan, M. Tinkham, R. M. Westervelt, and C. M. Lieber, Ge/Si nanowire mesoscopic Josephson junctions, *Nat. Nanotechnol.* **1**, 208–213 (2006).
- [39] J.-H. Choi, G.-H. Lee, S. Park, D. Jeong, J.-O. Lee, H.-S. Sim, Y.-J. Doh, and H.-J. Lee, Complete gate control of supercurrent in graphene p–n junctions, *Nat. Commun.* **4**, 2525 (2013).
- [40] D. Margineda, A. Crippa, E. Strambini, Y. Fukaya, M. T. Mercaldo, M. Cuoco, and F. Giazotto, Sign reversal diode effect in superconducting Dayem nanobridges, *Commun. Phys.* **6**, 343 (2023).
- [41] V. V. Ryazanov, V. A. Oboznov, A. Y. Rusanov, A. V. Veretenikov, A. A. Golubov, and J. Aarts, Coupling of two superconductors through a ferromagnet: Evidence for a π junction, *Phys. Rev. Lett.* **86**, 2427–2430 (2001).
- [42] H. Sickinger, A. Lipman, M. Weides, R. G. Mints, H. Kohlstedt, D. Koelle, R. Kleiner, and E. Goldobin, Experimental evidence of a φ Josephson junction, *Phys. Rev. Lett.* **109**, 107002 (2012).
- [43] C. T. Ke, C. M. Moehle, F. K. de Vries, C. Thomas, S. Metti, C. R. Guinn, R. Kallaher, M. Lodari, G. Scappucci, T. Wang, R. E. Diaz, G. C. Gardner, M. J. Manfra, and S. Goswami, Ballistic superconductivity and tunable π -junctions in insb quantum wells, *Nat. Commun.* **10**, 3764 (2019).
- [44] A. Assouline, C. Feuillet-Palma, N. Bergeal, T. Zhang, A. Motaghizadeh, A. Zimmers, E. Lhuillier, M. Eddrie, P. Atkinson, M. Aprili, and H. Aubin, Spin-orbit induced phase-shift in Bi_2Se_3 Josephson junctions, *Nat. Commun.* **10**, 126 (2019).
- [45] E. Strambini, A. Iorio, O. Durante, R. Citro, C. Sanz-Fernández, C. Guarcello, I. V. Tokatly, A. Braggio, M. Rocci, N. Ligato, V. Zannier, L. Sorba, F. S. Bergeret, and F. Giazotto, A Josephson phase battery, *Nat. Nanotechnol.* **15**, 656–660 (2020).
- [46] D. Margineda, J. S. Claydon, F. Qeivanaj, and C. Checkley, Observation of anomalous Josephson effect in nonequilibrium Andreev interferometers, *Phys. Rev. B* **107**, L100502 (2023).
- [47] G. Hutchinson, H. Qin, D. Hasko, D. Kang, and D. Williams, Controlled-junction superconducting quantum interference device via phonon injection, *Appl. Phys. Lett.* **84**, 136–138 (2004).
- [48] G. J. Podd, G. D. Hutchinson, D. A. Williams, and D. G. Hasko, Micro-squids with controllable asymmetry via hot-phonon controlled junctions, *Phys. Rev. B* **75**, 134501 (2007).
- [49] D. Drung and M. Mück, SQUID electronics, in *The SQUID Handbook* (2005) Chap. 4, pp. 127–170.
- [50] A. N. McCaughan and K. K. Berggren, A Superconducting-Nanowire Three-Terminal Electrothermal Device, *Nano Lett.* **14**, 5748–5753 (2014).
- [51] F. Giazotto and J. P. Pekola, Josephson tunnel junction controlled by quasiparticle injection, *J. Appl. Phys.* **97** (2005), 10.1063/1.1833576.
- [52] S. Tirelli, A. Savin, C. P. Garcia, J. P. Pekola, F. Beltram, and F. Giazotto, Manipulation and generation of supercurrent in out-of-equilibrium Josephson tunnel nanojunctions, *Phys. Rev. Lett.* **101**, 077004 (2008).
- [53] A. Morpurgo, T. Klapwijk, and B. Van Wees, Hot electron tunable supercurrent, *Appl. Phys. Lett.* **72**, 966–968 (1998).
- [54] J. Baselmans, A. Morpurgo, B. Van Wees, and T. Klapwijk, Reversing the direction of the supercurrent in a controllable Josephson junction, *Nature* **397**, 43–45 (1999).

Acknowledgments

This work was funded by the EU's Horizon 2020 Research and Innovation Framework Program under Grant Agreement No. 964398 (SUPERGATE), No. 101057977 (SPECTRUM), by the PNRR MUR project PE0000023-NQSTI, and by the PRIN project 2022A8CJP3 (GAMESQUAD).

Author contributions

D.M. fabricated the samples, conducted the experiments, and analyzed data with inputs from A.C., E.S., and F.G. The theoretical models were developed by Y.F., M.T.M., E.S., and M.C. The manuscript was written by D.M., A.C., and M.C., with inputs from all the authors. D.M., E.S., and F.G. conceived the experiment. F.G. supervised and coordinated the project. All authors discussed the results and their implications equally at all stages.

Competing interests

The authors declare no competing interests.

Additional Information

Supplementary Information The online version contains supplementary material.

Correspondence and requests for materials should be addressed to Daniel Margineda, Elia Strambini, and Francesco Giazotto.

SUPPLEMENTARY INFORMATION

Supplementary Note

Current-phase relation symmetries due to supercurrent back-action.

In this section, we will demonstrate that the back-action mechanism on the supercurrent i) will not produce any spontaneous phase, i.e. $I(\phi = 0) = 0$, and ii) rectification of the supercurrent will emerge for any functional form of the effective Josephson coupling $E_J(I)$ with an odd parity. To this aim, we start considering the free energy of a Josephson junction that can be cast into the form of

$$F_J = E_J[1 - \cos(\phi)]$$

with E_J the Josephson coupling and ϕ the phase difference among the superconductors forming the junction. For conventional configurations, E_J depends on factors related to the junction (e.g. material, barrier, etc). From the expression of the free energy, one can directly deduce the supercurrent flowing across the junction as the variation of the free energy with respect to the phase bias (in units of $\frac{2e}{\hbar}$):

$$I(\phi) = \frac{\partial F_J}{\partial \phi} \quad (1)$$

that yields the well-known Josephson relation $I(\phi) = I_c \sin(\phi)$ with $I_c = E_J$ being the critical current, namely, the maximal current that can sustain the junction without any voltage drop. This relation sets out the dc Josephson effect with a supercurrent existing between two superconductors that are coupled through a thin layer.

Now, we introduce the back-action mechanism on the amplitude of the supercurrent. We assume that the coupling among the superconductors depends on the amplitude of the supercurrent flowing across the junction. Hence, one can postulate a free energy of the type:

$$F_J = E_J(I)[1 - \cos(\phi)] \quad (2)$$

where the coupling $E_J(I)$ is a function of the supercurrent I flowing through the superconductors. Before discussing the structure of the coupling, we would like to emphasize that Eq. 2 describes a Josephson system with a transmission probability of Cooper pairs that depends on the amplitude of the supercurrent flowing across the junction. The form of F_J is consistent with the physical requirement that at zero applied phase bias ($\phi = 0$) the free energy is constant (i.e. $F_J(\phi = 0) = 0$) at any value of the supercurrent flowing through the junction. As a consequence, the self-induced supercurrent model fulfills the relation $I(0) = 0$, i.e. there is no spontaneous supercurrent flowing at zero phase bias. Such result can be deduced from the supercurrent expression obtained from Eq. 1 and Eq. 2:

$$I(\phi) = \frac{\partial E_J(I)}{\partial I} \frac{\partial I(\phi)}{\partial \phi} [1 - \cos(\phi)] + E_J(I) \sin \phi \quad (3)$$

There, by making the limit for $\phi \rightarrow 0$ on the two sides of the Eq. 3, the $I(0) = 0$ constraint is immediately deduced independently of the functional form for $E_J(I)$.

The second important feature refers to the connection between the back-action mechanism and the possibility of achieving a rectification of the supercurrent, i.e., the maximal positive forward amplitude turns out to be different from the maximal negative backward amplitude of the supercurrent.

For this issue, we consider the dependence of the Josephson coupling on the supercurrent amplitude in two different cases: i) $E_J(I)$ is an even parity function with respect to I , $E_J(-I) = E_J(I)$. ii) $E_J(I)$ is an odd parity function with respect to I , $E_J(-I) = -E_J(I)$.

In the first scenario, we can observe that for an effective coupling $E_J(I)$ with even parity, the solution for $I(\phi)$ will present a definite and odd parity with respect to ϕ , i.e. $I(\phi) = -I(-\phi)$. This conclusion can be deduced by analyzing the parity of Eq. 3 and constructing the solution in an iterative way with respect to the strength of the back-action amplitude coupling. Hence, for an effective coupling that has an even parity dependence in the supercurrent amplitude, the current phase relation yields a reciprocal transport.

In the second scenario ii), with $E_J(I)$ being an odd parity function with respect to I , the solution of the Eq. 3 will give a current phase relation that does not have a definite parity in the phase bias ϕ and therefore nonreciprocal transport. We can arrive to this conclusion without solving the self-consistent equations from the first derivative of the supercurrent

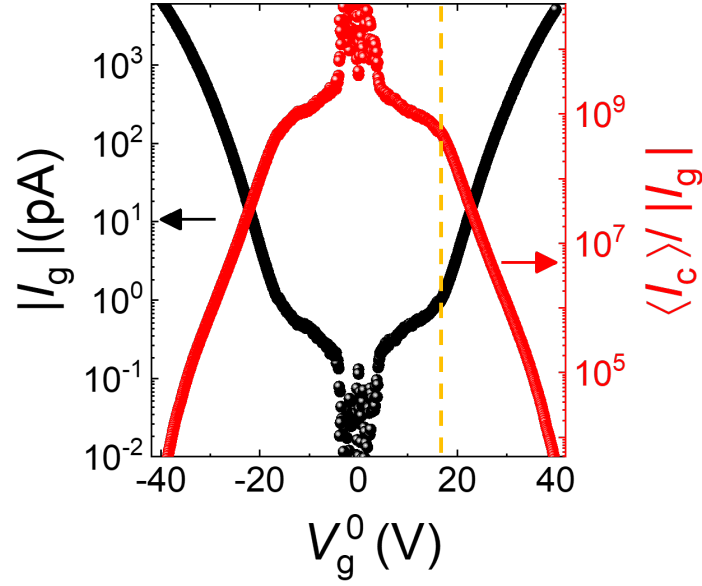
$$\frac{\partial I(\phi)}{\partial \phi} = \frac{I(\phi) - E_J(I) \sin(\phi)}{(1 - \cos \phi) \frac{\partial E_J(I)}{\partial I}}. \quad (4)$$

obtained from Eq. 3.

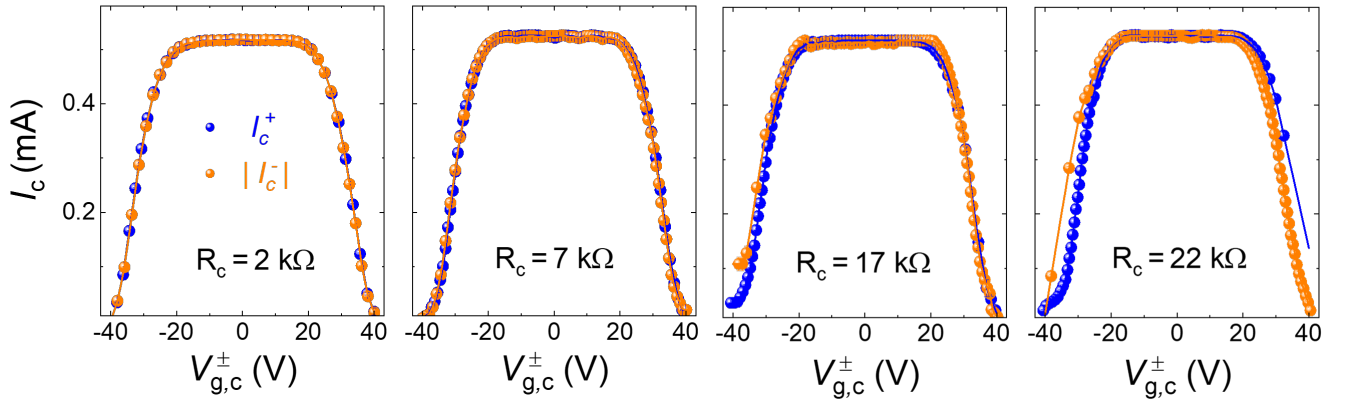
Maximum amplitude for the positive I_c^+ and negative I_c^- supercurrents is given by the condition $\frac{\partial I(\phi)}{\partial \phi} = 0$ (assuming that there are no discontinuities in the current phase relation). Since $I(\phi)$ does not have a definite parity in the variable ϕ , $I_c^+ = I(\phi_+) \neq I_c^- = I(\phi_-)$. This result implies that the supercurrent will be nonreciprocal for any functional form of the effective coupling $E_J(I)$ that includes odd parity terms with respect to the supercurrent amplitude I .

The model can be also extended to non-tunnel superconducting circuits in which the free energy may be more complex with respect to the simple cosine function. In particular, for reciprocal junctions, the cosine function will be substituted by a generic periodic even function, and through simple parity constraints the same conclusions can be extracted.

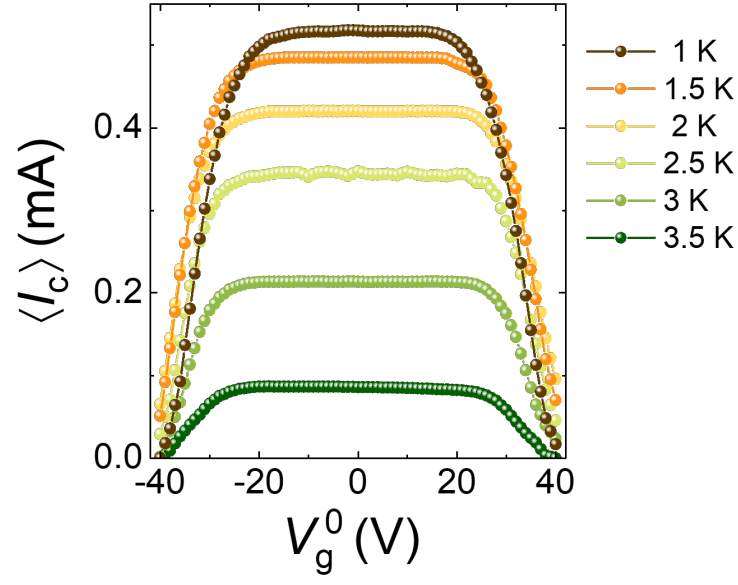
Supplementary Figures



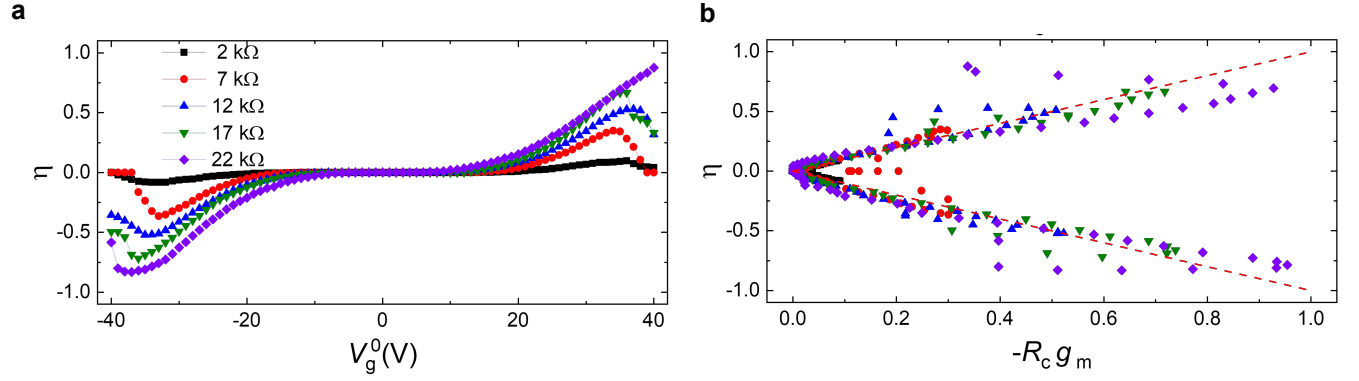
Supplementary Figure 1. Gate current. Gate-delivered leakage current to the weak link I_g at $T=1$ K (black dots). I_g increases from a few pA at the onset of the critical current $\langle I_c \rangle$ suppression (yellow dashed line) to a few nA at full suppression. $\langle I_c \rangle / I_g$ ratio is given by red dots.



Supplementary Figure 2. Back-action normalization. Quasi-symmetric behavior of the critical currents obtained by normalizing the gate voltage with the back-action contribution, $V_{g,c}^{\pm} = V_g - I_c^{\pm} R_c$ for different control resistors R_c .



Supplementary Figure 3. Temperature dependence of the gate-controlled supercurrent. Average critical current $\langle I_c \rangle$ as a function of the gate voltage V_g^0 for selected values of bath temperature.



Supplementary Figure 4. Diode rectification efficiency. **a**, Diode rectification parameter η as a function of the applied gate voltage V_g^0 for different control resistors R_c . **b**, η as a function of the back-action parameter $\alpha = -R_c g_m$ extracted from **a**, with the same color code. Negative rectification efficiency corresponds to negative gate voltages. Red dashed lines represent the ideal rectification $\eta = \alpha$ given by the linear model.